



Constraining the Internal Structures of Venus and Mars from the Gravity Response to Atmospheric Loading

Flavio Petricca¹, Antonio Genova¹, Sander Goossens², Luciano Iess¹, and Giorgio Spada³¹ Sapienza University of Rome, Department of Mechanical and Aerospace Engineering, Via Eudossiana 18, I-00184, Rome, Italy; flavio.petricca@uniroma1.it² NASA Goddard Space Flight Center, 8100 Greenbelt Road, Greenbelt, MD 20771, USA³ Dipartimento di Fisica e Astronomia, Università di Bologna, Viale Berti Pichat 8, Bologna, Italy

Received 2022 February 9; revised 2022 June 8; accepted 2022 June 12; published 2022 July 18

Abstract

The gravity fields of celestial bodies that possess an atmosphere are periodically perturbed by the redistribution of fluid mass associated with atmospheric dynamics. A component of this perturbation is due to the gravitational response of the body to the deformation of its surface induced by the atmospheric pressure loading. The magnitude of this effect depends on the relation between the loading and the response in terms of geopotential variations measured by the load Love numbers. In this work, we simulate and analyze the gravity field generated by the atmospheres of Venus and Mars by accounting for different models of their internal structure. By precisely characterizing the phenomena that drive the mass transportation in the atmosphere through general circulation models, we determine the effect of the interior structure on the response to the atmospheric loading. An accurate estimation of the time-varying gravity field, which measures the atmospheric contribution, may provide significant constraints on the interior structure through the measurement of the load Love numbers. A combined determination of tidal and load Love numbers would enhance our knowledge of the interior of planetary bodies, providing further geophysical constraints in the inversion of internal structure models.

Unified Astronomy Thesaurus concepts: [Planetary interior \(1248\)](#); [Planetary atmospheres \(1244\)](#); [Atmospheric tides \(118\)](#); [Tides \(1702\)](#); [Gravitational fields \(667\)](#)

1. Introduction

The terrestrial planets experience periodical mass redistributions driven by different mechanisms. Oceans, atmosphere, and continental water lead to significant mass transportation on Earth. On Venus and Mars, the mass distribution is only affected by atmospheric dynamics. The dominant contributions are thermal tides and the CO₂ cycle in the Venusian (Lebonnois et al. 2010, 2016) and Martian atmosphere (James et al. 1992), respectively. These dynamical effects yield temporal variations of the gravity field by transporting mass across the planet and causing a response of the body to the deformation of its surface induced by the fluid loading (Chao & Gross 1987; Boy et al. 2002).

Load-induced deformations and the consequent gravitational response depend on the planet's internal structure, and their effects are parameterized by the load Love numbers (Farrell 1972). Previous investigations of the gravitational effects of mass redistribution phenomena on Mars and Venus ignored its contribution by assuming no surface deformation (infinitely rigid interior; Karatekin et al. 2005; Sanchez et al. 2006; Bills et al. 2020). An initial assessment of the effects on Venus's gravity was given by Goossens et al. (2017a, 2019) using only degree 2 load Love numbers. The assumption of an infinitely rigid interior is well suited to study the atmospheric gravity signal with the latest solutions of the gravity field of Venus (Konopliv et al. 1999) and Mars (Genova et al. 2016; Konopliv et al. 2016). In these studies, only Genova et al. (2016) removed the gravity signal of the Martian atmospheric pressure cycle by precomputing its effects, leading to an accurate

estimation of the low-degree zonal gravity harmonics corrections associated with the carbon dioxide mass transportation between the polar caps. This approach allowed for straightforwardly disentangling the gravitational tidal effects between the atmosphere and the solid planet leading to a direct estimation of the tidal Love number k_2 related to the planet's interior.

A refined modeling of the gravitational contribution of the atmospheric dynamics will be fundamental to geophysical investigations of future space missions. Highly accurate radio science data will enable precise measurements of the static and time-varying gravity fields of the terrestrial planets. An independent model of the atmospheric gravity field will be required to thoroughly determine the gravitational anomalies associated with the solid planet only. The atmospheric gravity signal depends on the response of the solid planet to the surface loading that is measured by the load Love numbers (denoted with k'). These geophysical quantities thus provide information on the interior of the planet, and the combination of the load Love numbers with the tidal Love numbers can significantly constrain the inversion of the internal structure from geodetic observations. In addition, the combination of these quantities leads to the estimation of the tidal Love numbers associated with radial displacement (denoted with h). This study proposes a complementary measurement of h , which has always been the objective of dedicated laser or radar altimetry investigations. In the case of Venus, given the presence of a thick atmosphere and the relatively low amplitudes of the tidal deformations, measuring the tidal Love number h_2 is highly challenging, and the measurement of the load Love number k'_2 may be fundamental to revealing the interior structure of the planet.

In this work, we present the effects of the internal structure of Mars and Venus on the time-varying gravity field produced by their atmospheres. By using the numerical predictions of general circulation models (GCMs), we simulate the mass



Original content from this work may be used under the terms of the [Creative Commons Attribution 4.0 licence](#). Any further distribution of this work must maintain attribution to the author(s) and the title of the work, journal citation and DOI.

transportation that perturbs the gravity field of both planets. We then generate different interior models for the two planets and compute the resulting load Love numbers to investigate their impact on the atmospheric gravity fields.

This paper is organized as follows. In Section 2, we introduce the theoretical background of our work, including the methods to compute the gravity time variations from surface mass redistribution (Section 2.1), a description of the load Love numbers and their relation to the tidal Love numbers (Section 2.2), and a description of the methods we adopted to compute the viscoelastic load Love numbers (Section 2.3). In Section 3, we analyze the characteristics of the simulated atmospheric gravity fields of Mars and Venus (Section 3.1) and the effects of the internal structure on these gravity fields (Section 3.2). Finally, we provide a discussion of the results of our study in Section 4 and our conclusions in Section 5.

2. Methods

2.1. Time-varying Gravity Field from Surface Density Variations

The time-varying gravity field is used to account for the surface mass variations induced by the atmospheric dynamics. We express the gravity field in a spherical harmonics expansion (Kaula 1963) as follows:

$$U(r, \theta, \phi) = \frac{GM}{r} \left(1 + \sum_{l=2}^{+\infty} \left(\frac{R}{r} \right)^l \sum_{m=0}^l [C_{lm} \cos(m\phi) + S_{lm} \sin(m\phi)] P_{lm}(\sin \theta) \right), \quad (1)$$

where r , θ , and ϕ are the radial distance, latitude, and longitude in the planet body-fixed reference frame, respectively; R is the reference radius of the sphere; G is the gravitational constant; M is the mass of the planet; P_{lm} are the associated Legendre function of degree l and order m ; and C_{lm} and S_{lm} are the coefficients of the spherical harmonics expansion, also called Stokes coefficients. The time-dependent variations in the gravity field are represented in terms of variations of the spherical harmonics coefficients and denoted by ΔC_{lm} and ΔS_{lm} . According to Wahr et al. (1998), these are related to surface mass changes by

$$\Delta C_{lm} = \frac{3}{4\pi R \bar{\rho}} \frac{1 + k_l'}{2l + 1} \int \Delta \rho(r, \theta, \phi) P_{lm}(\sin \theta) \times \left(\frac{r}{R} \right)^{l+2} \cos(m\phi) \cos(\theta) d\theta d\phi dr, \quad (2)$$

where $\bar{\rho}$ is the mean density of the planet, k_l' is the load Love number of degree l (Farrell 1972), and $\Delta \rho(r, \theta, \phi)$ is the density variation caused by the mass transportation. The corresponding expression for ΔS_{lm} can be obtained by substituting $\cos(m\phi)$ in Equation (2) with $\sin(m\phi)$. In the approximation that the mass redistribution occurs in a thin layer, the density change is defined in terms of surface density:

$$\Delta \sigma(\theta, \phi) = \int \Delta \rho(r, \theta, \phi) dr. \quad (3)$$

The small thickness of the layer leads to approximately $\left(\frac{r}{R} \right)^{l+2} \simeq 1$, and Equation (2) turns out to be

$$\Delta C_{lm} = \frac{3}{4\pi R \bar{\rho}} \frac{1 + k_l'}{2l + 1} \int \Delta \sigma(\theta, \phi) \times P_{lm}(\sin \theta) \cos(m\phi) \cos(\theta) d\theta d\phi. \quad (4)$$

The surface mass density variations $\Delta \sigma(\theta, \phi)$ depend on the load considered. Wahr et al. (1998) presented a formulation for every loading phenomenon that takes place on Earth (i.e., oceanic, atmospheric, hydrological, and postglacial rebound). In this work, we focus on the influence of atmospheric mass transportation on the gravity field only, and $\Delta \sigma$ only accounts for the influence of the atmospheric dynamics. Since the atmosphere of the terrestrial planets is approximately in hydrostatic equilibrium, the change in the total mass can be integrated on a vertical column, yielding the pressure variations

$$\Delta P(\theta, \phi) = \Delta \sigma(\theta, \phi) g_0, \quad (5)$$

where g_0 is the mean gravity acceleration on the surface of the planet, and ΔP is the surface pressure anomaly caused by the atmospheric mass redistribution. As shown by Wahr et al. (1998), Equation (5) can be substituted into Equation (4), and ΔP can be expanded in spherical harmonics to obtain the time-dependent gravity coefficients,

$$\Delta C_{lm} = \frac{3}{R \bar{\rho} g_0} \frac{1 + k_l'}{2l + 1} \Delta C_{lm}^P, \quad \Delta S_{lm} = \frac{3}{R \bar{\rho} g_0} \frac{1 + k_l'}{2l + 1} \Delta S_{lm}^P, \quad (6)$$

where ΔC_{lm}^P and ΔS_{lm}^P are the spherical harmonics coefficients of the surface pressure variation fields. The term ΔC_{00} in Equation (6) is proportional to the variation of the total mass of the planet. All of the physical mechanisms responsible for the mass redistribution do not change the total mass of the planet, so ΔC_{00} is assumed equal to zero.

The time-varying part of the gravity field is characterized by amplitudes significantly lower with respect to the static field, limiting their estimation through radio science investigations to the lowest spherical harmonics degrees. The analysis of the highly accurate radio data of the GRACE mission (e.g., Tapley et al. 2004; Wahr et al. 2004) enabled the estimation of Earth's time-varying gravity field to degree and order 120 (Wouters et al. 2014). Space missions in orbit around Venus and Mars enabled the estimation of planetary gravity fields at lower resolutions compared to GRACE, leading to the observation of the temporal variations of the low-degree zonal harmonics on Mars only (e.g., Konopliv et al. 2011; Genova et al. 2016). Similar results should be expected from single satellite missions to Venus, since the determination of the high-degree harmonics would require dual-satellite missions similar to GRACE (e.g., Genova 2020; Genova & Petricca 2021).

2.2. Load Love Numbers

The planets and moons of the solar system continuously undergo body or surface external forcing applied by the interactions with other celestial bodies or by their fluid surface layers. The yielding of the body under the influence of an

external forcing is described in terms of radial and tangential displacements of its surface and changes in its gravitational potential. These induced deformations are related to the forcing by nondimensional Love numbers (Love 1911). Since the distortion mechanisms depend on the properties of the body, primarily its internal density, rigidity, and viscosity distributions, the Love numbers provide a unique insight into the interior of planets and moons. There exist three triplets of Love numbers that are sufficient to fully describe the response of a celestial body to any kind of forcing. Tidal Love numbers describe the response of a body to an external gravitational potential and are denoted by h, l, k . Load Love numbers quantify the response to a mass loading normal to the surface of the body and are denoted by h', l', k' . Finally, shear Love numbers characterize the response to a traction tangential to the surface and are denoted by h'', l'', k'' . Usually, k, k', k'' relate the forcing to the induced potential variation, while h, h', h'' and l, l', l'' express the relations between the external forcing and the radial and tangential displacements of the surface, respectively.

If a viscoelastic body is subjected to a periodic forcing (e.g., gravitational tides and atmospheric loading acting on the terrestrial planets), the Love numbers and response depend on the frequency of the forcing. This dependence is quantified by the rheology of the internal layers. Conversely, the response and Love numbers of a fully elastic body can be assumed independent on the frequency of the perturbation in the limit of quasi-static deformations, i.e., when the frequency of the forcing is not significantly high (Takeuchi & Saito 1972; Saito 1974).

Love numbers are usually represented in spherical harmonics to determine their dependency on long- and short-wavelength spatial scales. The Love numbers of degree $l=1$, for example, in Equation (6) yield variations of the position of the center of mass. Since the origin of the gravity field reference frame coincides with the center of mass of the planet, the degree 1 load Love number is equal to -1 , and all ΔC_{1m} and ΔS_{1m} are zero (Equation (6)). This assumption is valid even if the planet has an atmosphere. The position of the solid planet's center of mass changes according to the atmosphere mass redistribution to enable an unperturbed instantaneous center of mass of the system solid planet plus atmosphere. For an extensive review of the relation between the reference frames and the load Love numbers, see Blewitt (2003). Our results are based on a reference frame whose origin coincides with the system solid planet plus atmosphere center of mass, and we assume $k_1^l = -1$.

The three sets of Love numbers show lower magnitudes at higher harmonic degrees, approaching an asymptotic value close to zero. The influence of the load Love numbers is thus limited to the lower degrees of the harmonic expansion of the time-varying gravity field. The Love number sets are tied through different constraints (Saito 1978), as, for example,

$$k' = k - h. \quad (7)$$

Gravity and radio science investigations enabled accurate measurements of the tidal Love number k_2 for many celestial bodies in the solar system, including the Moon (e.g., Konopliv et al. 2013; Lemoine et al. 2014), Mars (e.g., Genova et al. 2016; Konopliv et al. 2016), Mercury (e.g., Mazarico et al. 2014; Verma & Margot 2016; Genova et al. 2019; Konopliv et al. 2020), Venus (e.g., Konopliv & Yoder 1996), and Titan (e.g., Iess et al. 2012). These estimates were obtained by disentangling the tidal gravitational response from the static

gravity field. The measurements of the tidal Love numbers have been used as constraints for the inversion of the interior structure, providing important information on the properties of the celestial bodies. Observations of the gravitational tides on the Moon and Mars provided the geodetic evidence that they possess a liquid or partially liquid core (Yoder et al. 2003; Khan et al. 2004). The detection of Titan's gravitational tides is consistent with a global subsurface ocean (Iess et al. 2012) and informs on its density and thickness (Baland et al. 2014; Mitri et al. 2014).

Given the weakness of the atmospheric gravity signal and the radiometric data accuracy of the previous missions, the load Love numbers have not been observed yet. The retrieval of the load Love numbers through future investigations in the solar system would yield an additional constraint on the internal structure of planets and moons that possess an atmosphere. In addition, by combining the k and k' measurements, tidal deformations can be indirectly determined by computing the tidal number h through Equation (7). This result would extend the scientific return of gravity studies, providing a complementary recovery of the radial displacement induced by gravitational tides that is an objective of altimetry investigations.

2.3. Computation of Viscoelastic Load Love Numbers

To assess the influence of the internal structure on the atmospheric gravity field, we explored a range of load Love numbers by generating a series of interior models of Venus and Mars. The density and rigidity reference profiles used in this study are based on the works by Dumoulin et al. (2017) and Khan et al. (2018) for Venus and Mars, respectively (see Section 3.2). The software ALMA (Spada & Boschi 2006; Spada 2008) was used to determine the tidal and load Love numbers for each internal structure by assuming a spherically symmetric and incompressible planet. A model of the planet is supplied to ALMA by providing the density, rigidity (shear modulus), and viscosity radial structure and defining the rheology of the internal layers. ALMA computes the Love numbers of the body by adopting the viscoelastic normal modes method (Peltier 1974) based on the solution of the equilibrium problem in the Laplace domain through the propagator matrix approach. ALMA can also provide the frequency-dependent Love numbers that describe the response to a periodic forcing, such as gravitational tides and atmospheric loading. The tidal and loading forcing are modeled by a sinusoidal function in the frequency domain. By specifying the period of the forcing and a planetary interior model, we are able to compute the frequency-dependent load Love numbers.

We also investigate the impact of the internal rheology of the planet on the load Love numbers, accounting for dissipation processes that are neglected when the response of the planet is assumed to be purely elastic. This assumption is acceptable for most of the loads that act on the surface of the Earth where the surface loading occurs at relatively short timescales, including those related to the atmospheric dynamics. This is not the case for the other terrestrial planets. The deformations caused by the Venusian atmospheric thermal tides occur on a timescale dictated by the planet rotation, whose period is 116.75 Earth solar days. The carbon dioxide cycle on Mars has a period of 1 Martian yr (687 Earth solar days). In both cases, the deformations are characterized by relatively long timescales,

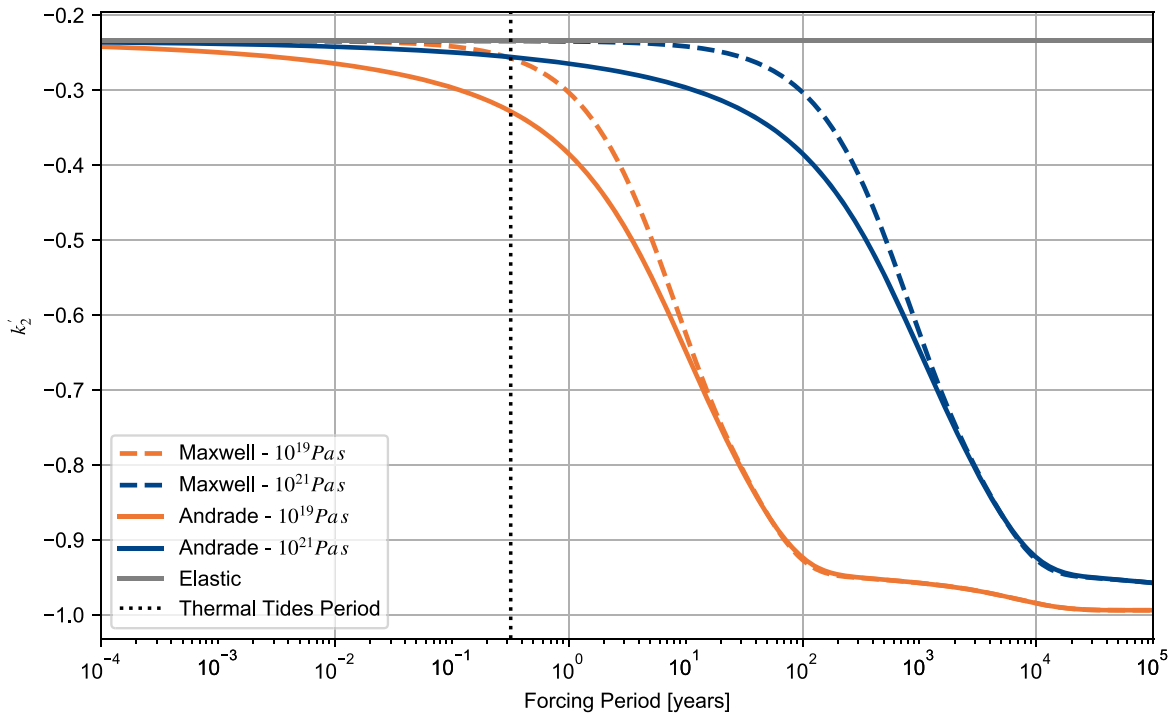


Figure 1. Degree 2 load Love number of Venus’s dependence on the frequency of the loading by assuming different rheology models. The dotted line represents the period of the thermal tides responsible for the loading deformations on Venus.

and the viscoelastic dissipation may have a significant influence.

To explore the sensitivity of the load Love numbers to the viscoelastic dissipation, a rheological model of the planet interior is adopted among those developed through laboratory-based experiments. A thorough review of these models and their planetary application is presented in Castillo-Rogez et al. (2011) and Bagheri et al. (2019). Bagheri et al. (2019) recommended the use of the Andrade (Andrade 1910), extended Burgers (Jackson & Faul 2010), or Sundberg–Cooper (Sundberg & Cooper 2010; Renaud & Henning 2018) models because they are able to reproduce the anelastic transient response that connects the fully elastic regime with the pure viscous response, while the simpler Maxwell model includes the elastic and viscous regimes only. The Maxwell model has been extensively used for Earth applications as a very good approximation of long-period deformations such as those associated with the postglacial rebound (Peltier 1974). For Mars, the Maxwell model was used to fit the observation of Phobos’s secular acceleration due to gravitational tides and infer the viscosity of the mantle (Bills et al. 2005). However, this viscosity value is very low (2×10^{16} Pa s), while the Andrade model enables a fit of the same data with a viscosity value that is in the expected range of 10^{19} – 10^{22} Pa s (Bagheri et al. 2019). The viscosity of the Martian mantle was also investigated by Samuel et al. (2019) by analyzing the coupling between the thermal history of Mars’ interior and the orbital evolution of Phobos, suggesting a viscosity value higher than that inferred by Bills et al. (2005) with the Maxwell model.

The period of the atmospheric mass transportation phenomena causing time variations of the gravity fields of Venus (1 Venus solar day) and Mars (1 Martian yr) can be assumed as intermediate between those of the short-period seismic waves and the long-period tides. Previous investigations assumed a transient rheology to model the viscoelastic response to the

tidal deformations of the terrestrial planets, including Mars (Nimmo & Faul 2013), Venus (Dumoulin et al. 2017), and Mercury (Padovan et al. 2014). Since the period of the loading deformations is longer than the period of the tidal deformations for Mars and Venus, the employment of a transient viscoelastic rheology is appropriate to model the response of both planets to the atmospheric loading. Therefore, we use the Andrade model for the mantle of both planets with a creep function (i.e., a relation between the response of the material and the forcing in the time domain) composed of the elastic, viscous, and transient terms. The response is usually described in the frequency domain through the Laplace transform of the creep function, called the complex compliance. The inverse of the complex compliance is the complex shear modulus. For the Andrade model, the complex compliance $J(\omega)$ for a periodic forcing is

$$J(\omega) = \frac{1}{\mu} - \frac{j}{\eta\omega} + \beta(j\omega)^{-\alpha}\Gamma(1 + \alpha), \quad (8)$$

where μ is the elastic shear modulus, η is the viscosity, Γ is the gamma function, ω is the frequency of the forcing (i.e., the atmospheric loading for the case analyzed in this work), and α and β are the parameters that characterize the frequency dependence of the transient term. Following the approach illustrated by Castillo-Rogez et al. (2011) and used by Dumoulin et al. (2017), we assume $\beta = \mu^{\alpha-1}\eta^{-\alpha}$; the value of α is between 1/5 and 1/3. We assume a value of 0.3 for both Venus and Mars.

To show the differences between a fully elastic and a viscoelastic response, we computed the degree 2 load Love number of Venus by varying the frequency of the forcing and assuming different models for the mantle. Figure 1 shows the dependence of k_2' on the period of the forcing when the

Andrade and Maxwell models are used to model the mantle of Venus.

Significant differences are observed at the timescale of the loading deformations induced by the thermal tides. The deviation from an elastic response is enhanced as the viscosity of the mantle decreases. This behavior is amplified for the Andrade model by the transient components of the rheology that affect the response to the atmospheric loading on the timescale intermediate between the fully elastic and viscous regimes.

3. Atmospheric Loading and Internal Structure Response

3.1. Atmospheric Gravity Field

To evaluate the time-varying gravity field generated by the atmospheres of Venus and Mars, we simulated the different mass transportation phenomena that act on the two planets. We ran GCM simulations to compute surface pressure grids, and we evaluated the pressure anomaly ΔP as follows:

$$\Delta P(t, \theta, \phi) = P(t, \theta, \phi) - \bar{P}(\theta, \phi), \quad (9)$$

where $P(t, \theta, \phi)$ is the surface pressure grid at each time step of the GCM simulation, and $\bar{P}(\theta, \phi)$ is the temporal average of the surface pressure grids. The anomaly is then expanded in spherical harmonics, and the gravity time variations are computed according to Equation (6).

3.1.1. Venus's Thermal Tides

An accurate model of Venus's GCM released by the Institute Pierre-Simon Laplace (IPSL; Lebonnois et al. 2016; Garate-Lopez & Lebonnois 2018) is used to simulate the mass redistribution. This model is computed on a grid with a resolution of $1^\circ 875$ in latitude and $3^\circ 750$ in longitude. It accounts for the contribution associated with the surface height based on the planetary topography, the soil type, and a full radiative transfer module. As described in Section 2, the surface mass variations can be assumed to be localized in a thin layer close to the surface so that they can be expressed through variations in surface pressure. Since the atmospheric thermal tides are the dominant contribution and characterized by the longest period, we simulated the atmospheric dynamics for one period of this phenomenon that corresponds to 1 Venusian solar day (116.75 Earth days). We ran the GCM for 1 Venusian solar day, sampled the output surface pressure fields, and expanded all of the grids in spherical harmonics to include all of the contributions to the atmospheric mass transportation. As shown in Bills et al. (2020), the thermal tides are the main drivers of Venus's atmospheric gravity field time variations, but not the only ones. An analysis of all of the atmospheric waves simulated by the IPSL Venus GCM is presented in Lebonnois et al. (2016). Most of the waves are characterized by a smaller spatial scale than that of the planetary-scale thermal tides, and they affect the short-wavelength terms of the gravity field (i.e., high-degree harmonics). We sampled the pressure fields to include both low-frequency thermal tides and high-frequency terms with smaller spatial scales by using a sampling time of 1 Earth solar day, leading to 117 samples.

The spatial patterns of the time-varying gravity fields are usually reported in terms of the involved geoid temporal changes ΔN (e.g., Wahr et al. 1998), which are computed as

follows:

$$\Delta N = R \sum_{l=0}^{+\infty} \sum_{m=0}^l [\Delta C_{lm} \cos(m\phi) + \Delta S_{lm} \sin(m\phi)] P_{lm}(\sin \theta). \quad (10)$$

Figure 2 shows the geoid temporal variations induced by the atmosphere at four different times, equally spaced throughout the Venus solar day. The sum in Equation (10) is truncated at $l = 40$, which provides a sufficient spatial resolution to capture both the large- and small-scale atmospheric dynamics.

The sectorial pattern of these geoid variations is due to the thermal tides that are the dominant effect on the gravity field and rotates in phase with the subsolar point. The sectorial harmonics (i.e., coefficients with $l = m$ in Equation (1)) are larger than the zonal harmonics (i.e., coefficients with $m = 0$ in Equation (1)), which are longitude-independent and, therefore, characterized by a lower sensitivity to the zonal circulation induced by the thermal tides. This is shown in Figure 3, which displays the temporal variations of the degree 2 zonal and sectorial harmonics.

The ΔC_{22} term, which is the harmonic with the greatest amplitude, shows a large signature associated with the thermal tides, since its time variations are dominated by a periodicity of 1 Venus solar day. The high-frequency variations are due to the other atmospheric waves, which are characterized by frequencies up to 30 cycles per Venus solar day (Lebonnois et al. 2016). The peak-to-peak geoid change induced by ΔC_{22} is about 0.5 cm. For comparison, Leuliette et al. (2002) computed an amplitude of the atmospheric ΔC_{22} for the Earth, which is an order of magnitude lower ($\sim 0.4 \times 10^{-10}$, corresponding to geoid variations of ~ 0.03 cm) compared to our Venus predicted value based on the IPSL GCM. Venus high-pressure variations lead to a significant load on the surface at the Venusian solar day timescales.

Our modeling of the thick atmosphere of Venus as a thin atmospheric layer is acceptable whether the spherical harmonic of degree l fulfills the following relation (Wahr et al. 1998):

$$(l + 2) \frac{H}{R} \ll 1, \quad (11)$$

where H is the thickness of the layer, and R is the mean radius of the planet (6051 km). By assuming that the greatest part of the atmospheric mass is within one scale height ($H = 15.9$ km) and an upper threshold for the first member of Equation (11) of 0.1, the maximum degree for which the thin shell assumption is valid is ~ 36 . Any higher-degree coefficient may be affected by errors due to the simplified model. This upper bound in spherical harmonic coefficients is well suited for our purposes because, as shown in Section 3.2, harmonic degrees greater than 4 present very limited sensitivity to the internal structure of the planet. A technique to extend the model to account for the three-dimensional structure of the atmosphere is presented in Boy & Chao (2005).

3.1.2. Martian CO₂ Cycle

The most important mechanism that causes large-scale mass redistribution in the atmosphere of Mars is the carbon dioxide exchange between the polar caps. This seasonal cycle is generated by the sublimation of the CO₂ ice at the summer pole and is responsible for the transportation of 25%–30% of the total atmospheric mass from one pole to the other during

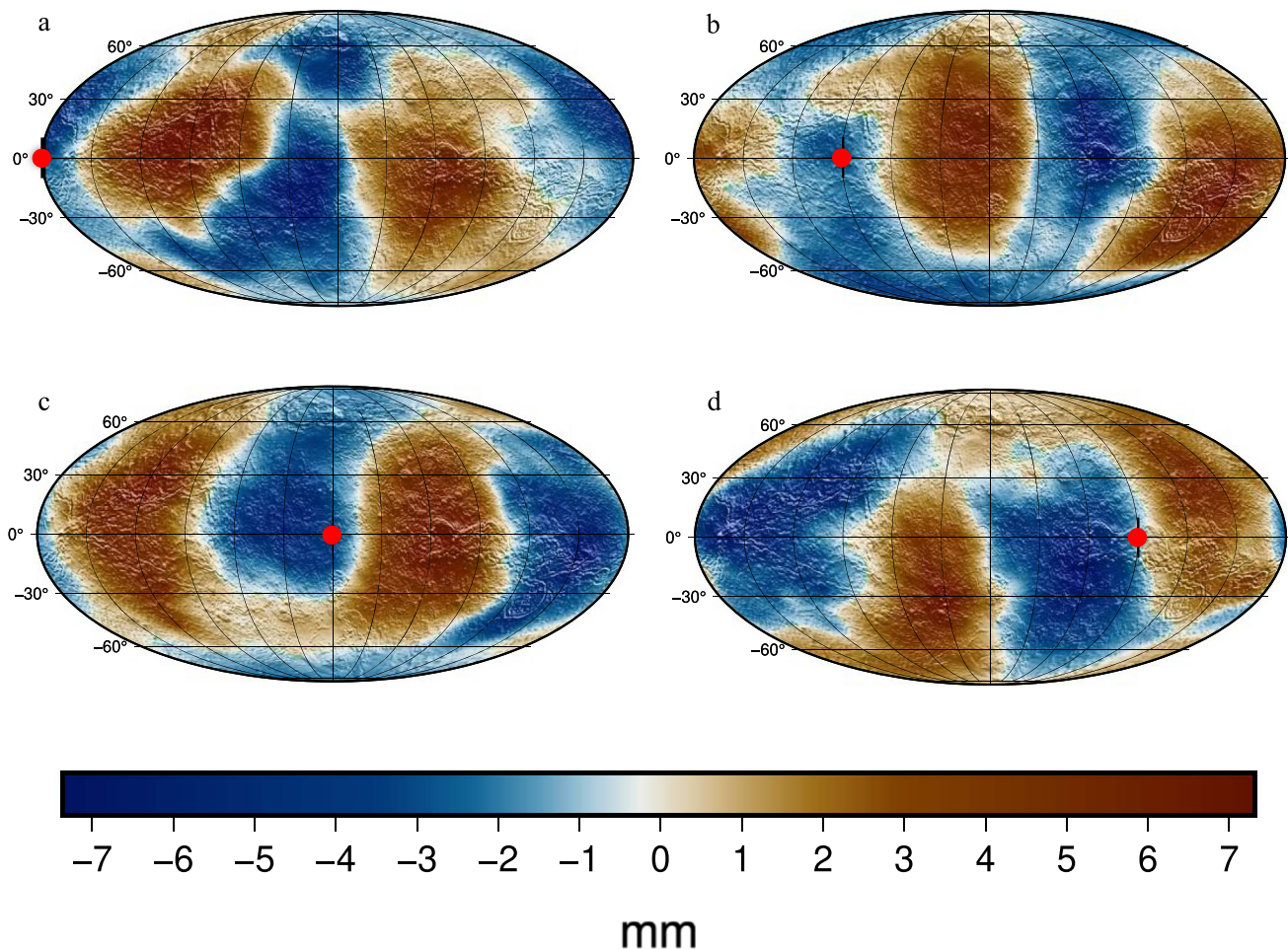


Figure 2. Temporal variations of the Venus geoid induced by the atmosphere over shaded topographic relief at four different times. The maps are centered at 180° longitude. The subsolar point (red dot) is located at longitude (a) 0°, (b) 90°, (c) 180°, and (d) 270°. The visible sectorial pattern is produced by the thermal tides and rotates in phase with the subsolar point.

the Martian year (e.g., James et al. 1992; Smith et al. 1999). The diurnal cycle originated by the thermal tides is significantly lower compared to Venus’s atmosphere (Wilson & Hamilton 1996). The topography also has a strong impact on Mars’ pressure field through the north–south dichotomy (Hourdin et al. 1993).

Simulations of the atmospheric circulation of Mars were carried out with the Mars global reference atmospheric model 2010 (Justh et al. 2011) for 1 Martian yr by using a time step of 2 hr. Pressure field grids were generated with the same resolution of the Venus case. In this case, a large portion of the mass transportation occurs poleward, because the greatest contribution is given by the exchange of CO₂ between the two polar caps. Since the spatial pattern of this mass redistribution mainly perturbs the zonal harmonics of the gravity field, the amplitudes of the time-varying zonal harmonics are substantially larger than those of the sectorial harmonics. Figure 4 shows the degree 2 zonal and sectorial harmonics for 1 Martian yr with a zoom in over 2 solar days. Our simulation starts at the spring equinox of the northern hemisphere.

The thermal tides on Mars lead to gravitational effects with diurnal and semidiurnal frequencies, as shown in the zoom in on Figure 4. The amplitudes of the daily-varying ΔC_{22} term range between -6×10^{-11} and 3×10^{-11} , corresponding to

-0.2 and 0.1 mm in geoid displacements, which are significantly lower compared to the Venus daily gravity variations induced by the thermal tides.

The main time-varying gravity signal of Mars is associated with the annual pressure cycle that produces larger variations in the zonal harmonics. The ΔC_{20} strongly increases at 270° areocentric longitude, which is the winter solstice of the northern hemisphere. Although Venus has pressure and mass variations about 1 order of magnitude larger than Mars, their gravity variations induced by the atmosphere are comparable. This can be explained by observing that the gravity perturbation is a function of the ratio between the mass variation and the planet’s total mass, as shown in Equation (4).

3.2. Internal Structure Response to Atmospheric Loading

To retrieve the contribution of the internal structure to the atmospheric gravity field, we computed ensembles of interior models by accounting for different properties of the mantle and core, assumed to be entirely liquid or entirely solid. This assumption was supported by tests dedicated to studying the effects of the presence of a solid inner core on the degree 2 tidal and load Love numbers. For Venus, we used the same structure predicted by the preliminary reference Earth model (PREM; Dziewonski & Anderson 1981) for the Earth’s inner core, with

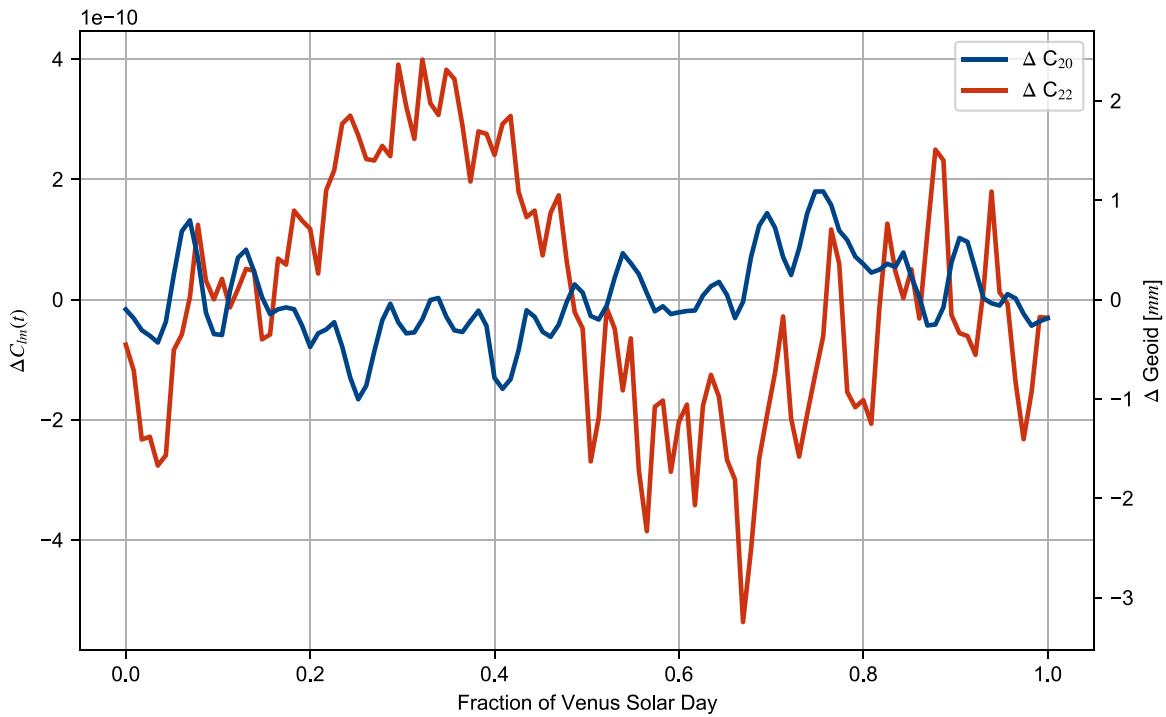


Figure 3. Time variations of the degree 2 zonal and sectorial gravity field harmonics due to the atmospheric mass redistribution during a Venus solar day. The spherical harmonics coefficients are 4π normalized.

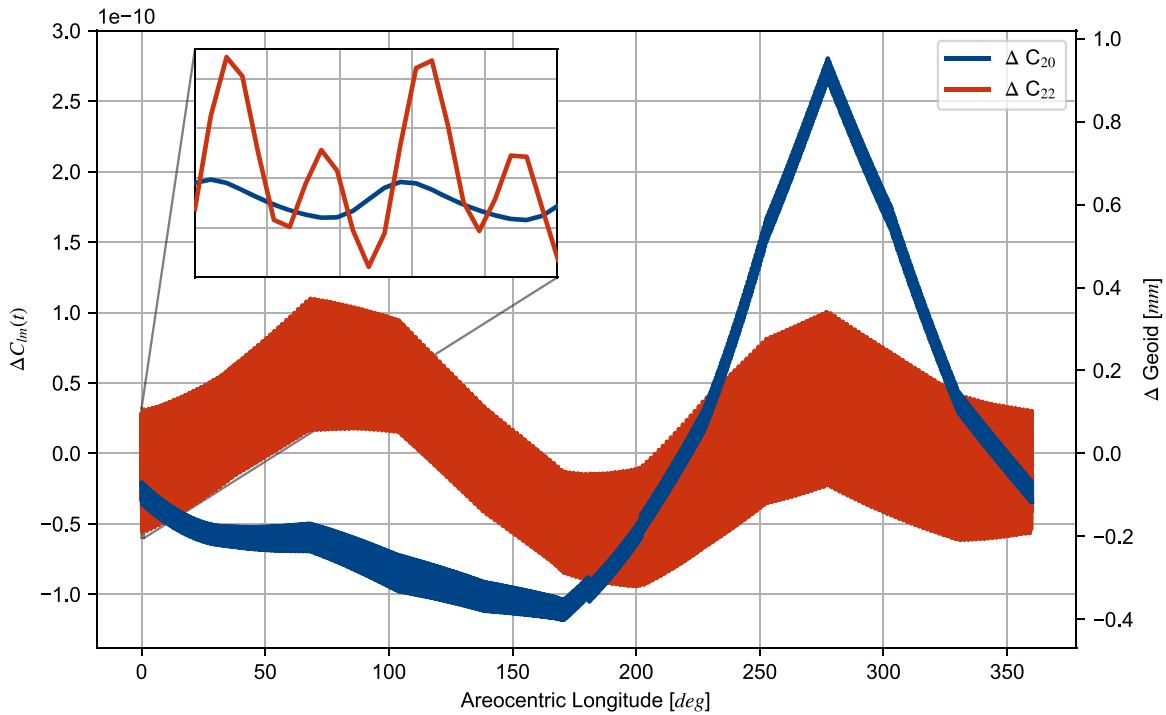


Figure 4. Variations of the degree 2 zonal and sectorial gravity field harmonics due to the atmospheric mass redistribution during a Martian year. The spherical harmonics coefficients are 4π normalized.

a radius of 1228 km. For Mars, the radius of the solid inner core was varied in the range 100–1228 km. In both cases, the influence of the solid inner core is negligible. This is consistent with previous investigations that suggested a minor contribution of the core differentiation to the tidal Love number k_2 (e.g., Padovan et al. 2014 for the case of Mercury).

The density and rigidity (shear modulus) profiles used to generate our models are based on Dumoulin et al. (2017) and Khan et al. (2018). We selected the V5 model by Dumoulin et al. (2017) for Venus and the TAY model by Khan et al. (2018) for Mars as reference profiles. We fit a third-degree polynomial to the reference profiles to extrapolate the density

Table 1
Range of Interior Properties for the Internal Structure Models of Venus and Mars

		Density (kg m^{-3})	Rigidity (GPa)	Viscosity (Pa s)	Rheology
Venus	Core	10098.17–11024.78	99.58–121.42	10^{11} – 10^{20}	Fluid, Andrade
	Lower mantle	4390.30–4894.14	193.23–235.81	10^{19} – 10^{22}	Elastic, Andrade
	Upper mantle	3323.92–3959.01	81.60–97.05	10^{19} – 10^{22}	Elastic, Andrade
	Crust	2950.00	30.20	...	Elastic
Mars	Core	6165.98–6400.51	Fluid
	Mantle	3423.15–3589.45	71.96–77.82	10^{19} – 10^{22}	Elastic, Andrade
	Crust	2582.00	20.24	...	Elastic

and rigidity to different core structures. To compute the Love numbers, ALMA requires the discretization of the planet into homogeneous layers. Therefore, we average the extrapolated density and rigidity profiles to generate three-layer models for Mars (core, mantle, and crust) and four-layer models for Venus, accounting for a lower and an upper mantle. The transition between the lower and upper mantle is approximated to occur at a depth of 670 km for all models, as described by the PREM model for the Earth (Dziewonski & Anderson 1981). The density and rigidity of each layer are assumed to be constant. Variations in the core size with respect to the reference models lead to variations in total mass, which need to be balanced in order for the model to be compliant with the observed total mass of the planet. For each model, we compute the mass balance equation for a three- or four-layer planet. By specifying the variations in the core–mantle boundary radius with respect to the reference model, we determine the constant density offset required to balance the induced mass variations. This offset is then used to adjust the core and mantle density to provide the final density structure, which is compliant with the total mass constraint.

Each model is characterized by a different rheology, size, and viscosity of the core and rheology and viscosity of the mantle. The viscosity in the core and mantle is assumed to be constant for both planets. A new model is generated by specifying a full set of these properties and accounting for the total mass of the planet as a constraint. A further criterion to accept the resulting interior model is associated with the measured moment of inertia (MoI). For each internal structure, we compute the MoI of the model to assess whether it is consistent within three times the standard deviation (3σ) of the geophysical measurements retrieved by Margot et al. (2021) for Venus and Konopliv et al. (2016) for Mars. The models that do not meet this requirement are then discarded.

The ranges of values adopted for the generation of interior models are presented in Sections 3.2.1 and 3.2.2 and reported in Table 1. Our results are not significantly affected by the choice of the reference profiles from Dumoulin et al. (2017) and Khan et al. (2018), since we explore a very broad range of core and mantle properties to compute the Love numbers. The end-members of the core and mantle density and rigidity in Table 1 correspond to the models with the smallest and largest core size. For both Mars and Venus, the shear modulus of the liquid core is zero. For the case of the Venus solid core, the rigidity profiles were extrapolated from the Earth’s inner core structure predicted by the PREM model as in Dumoulin et al. (2017).

The crustal properties were not varied in our analysis, since this thin layer does not significantly affect our results regarding the low-degree gravity field. In addition to the total mass and MoI constraints, we also constrained this generation of planetary interior models by requiring that the computed tidal

Love number k_2 is in agreement with the measurements obtained by Konopliv & Yoder (1996) for Venus and Genova et al. (2016) and Konopliv et al. (2016) for Mars. Since these observations are mainly based on the gravitational tides induced by the Sun, the tidal Love numbers are computed at frequencies corresponding to the period of the solar semi-diurnal tides, that is, 12 hr and 19 minutes for Mars and 58 days and 8 hr for Venus. On the other hand, the dominant contribution to the surface loading is given by the thermal tides for Venus and the CO_2 cycle for Mars; therefore, we compute the load Love numbers at the frequencies of these phenomena, corresponding to a period of 116 days and 16 hr for Venus and 687 days for Mars.

The load Love numbers of Mars were first computed by Metivier et al. (2008) by assuming a purely elastic model to investigate the connection between the internal structure of the planet and its seasonal deformation. The loading deformations and load Love numbers of Venus are still unknown and poorly investigated.

3.2.1. Venus

Venus’s internal structure is uncertain, since our knowledge of the main geophysical parameters is still not accurate enough to constrain the size and rheology of the planet’s core. Dumoulin et al. (2017) showed that the observed k_2 would rule out the possibility of an entirely solid core only if the response of the planet to the gravitational tides is assumed to be purely elastic. However, an internal structure that includes a completely solid core would still enable a match with the observed k_2 if viscoelastic effects are accounted for. In our simulations, we included models with a fully fluid inviscid core and an entirely solid viscoelastic core, modeled through the Andrade rheology (see Section 2.3). As in Dumoulin et al. (2017), the viscosity of the core was varied in a range whose end-members are consistent with the values of the Earth’s inner core inferred through either geophysical modeling or laboratory experiments. The experiment-based approaches lead to a large uncertainty on the viscosity of the core ranging from 10^{11} (Van Orman 2004) to 10^{20} (Reaman et al. 2012) Pa s. Geodynamic modeling provides a viscosity in agreement with this range (e.g., 3×10^{17} Pa s; Davies et al. 2014). The viscosity of Venus’s core is then varied within 10^{11} – 10^{20} Pa s. Regarding the size of the core, we explored a broad range of values, from 2800 to 3600 km. For the mantle of Venus, we used both a purely elastic and an Andrade rheology. In the latter case, we assumed a mean viscosity for the mantle ranging between 10^{19} and 10^{22} Pa s, which is the interval of values expected for the mantle of the Earth. On top of these layers, we assume an elastic crust characterized by a density of 2950 kg m^{-3} and a mean thickness of 60 km in line with Dumoulin et al. (2017).

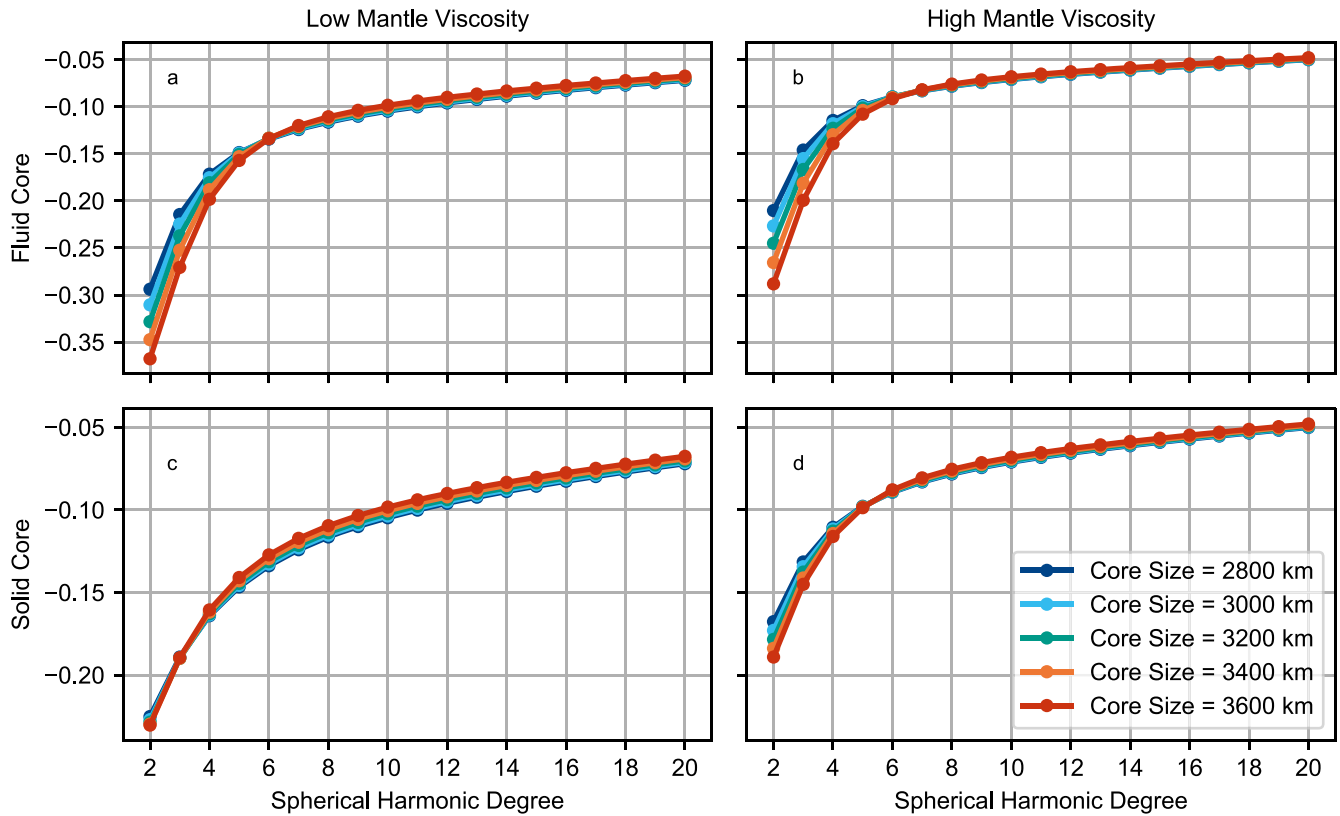


Figure 5. Load Love numbers of Venus up to degree 20 for different interior models. The core is assumed to be entirely fluid in panels (a) and (b) and entirely solid in panels (c) and (d). Models in panels (a) and (c) are characterized by low mantle viscosity (10^{19} Pa s), and a higher value (10^{22} Pa s) is selected for panels (b) and (d).

The load Love numbers are computed for each of the models generated. All of the models that yielded a computed degree 2 tidal Love number outside a confidence interval of three standard deviations from the estimate by Konopliv & Yoder (1996) were discarded. Figure 5 shows the load Love numbers of Venus up to degree 20 for an entirely liquid (Figures 5(a)–(b)) and solid (Figures 5(c)–(d)) core as a function of the core radius for two different mantle viscosities (a low value of 10^{19} Pa s and a higher value of 10^{22} Pa s). In the case of the solid core, its viscosity is fixed at 10^{18} Pa s.

Interior models show lower load Love numbers with increasing sizes of the core, and this sensitivity to the core radius is enhanced for fluid cores. Higher viscosities of the mantle lead to higher load Love numbers. The variations at low degrees are mostly due to the relative size of the solid or liquid core and to the mantle viscosity. At degrees l larger than 5, the mantle viscosity has a major impact on the gravity response to surface loading, while the core size has a negligible effect. A negative load Love number implies that the deformation of the planet’s surface dampens the atmospheric gravitational perturbation. A liquid core or a mantle with low viscosity would amplify this damping effect because of the lower rigidity of the planet.

A detailed analysis of the degree 2 load Love numbers is presented in Figures 6 and 7 by assuming a fluid inviscid and solid core, respectively. We present k_2^l for different models to show the sensitivity of the load Love number to the properties of the interior structure. Crosses indicate models that do not fulfill the requirement related to the agreement between the computed and observed k_2 . Gray dots represent models with a fully elastic mantle.

The load Love numbers decrease with the radius of the liquid core as the deformability of the planet increases, and the gravitational perturbation is attenuated. Low mantle viscosities further contribute to increase the absolute value of k_2^l by $\sim 30\%$. This is the difference computed between an elastic model and a model with a low mantle viscosity.

The differences between elastic and viscoelastic models are even higher when the anelastic dissipation of the core is accounted for. Figure 7 shows the degree 2 load Love number for all of the accepted models with a fully viscoelastic solid core. In this case, the absolute value of the load Love numbers is lower with respect to the fluid core case, inflating the atmospheric effects on the gravity field. The sensitivity of the load Love numbers to the viscosity of the core is high, yielding differences between two end-members of up to $\sim 50\%$ for a large core. This sensitivity is increased for larger sizes of the core. However, the load Love numbers become rather insensitive to any change in the viscosity of the core when this is lower than 10^{16} Pa s or higher than 10^{19} Pa s.

The k_2^l for all of the accepted models is in the range between -0.340 and -0.165 , which yields variations up to 24% in the time-varying harmonics of degree 2 among different models. Higher harmonics are also affected by the internal structure of the planets. The k_3^l for models that we generated is in the range including -0.229 and -0.127 , while the k_4^l varies between -0.168 and -0.105 . This corresponds to differences in the degree 3 and 4 harmonics of about 13% and 7%, respectively. Spherical harmonics degrees greater than 5 are less sensitive to the internal structure, with variations lower than 5%. The inclusion of viscoelastic effects in our modeling of Venus’s internal structure results in a broader range of possible degree 2

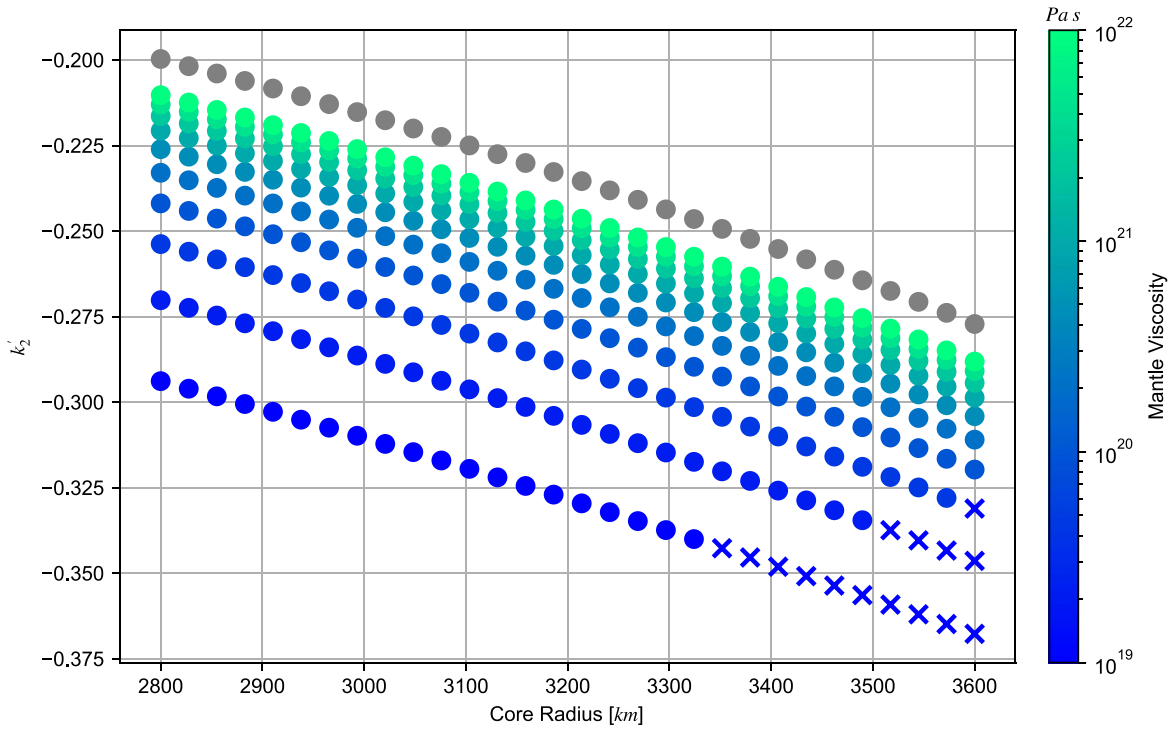


Figure 6. Degree 2 load Love number of Venus for models with a fluid inviscid core and varying core size and mantle viscosity. Crosses represent models for which the computed k_2 is not in agreement with the observations. Gray dots represent models with an elastic mantle.

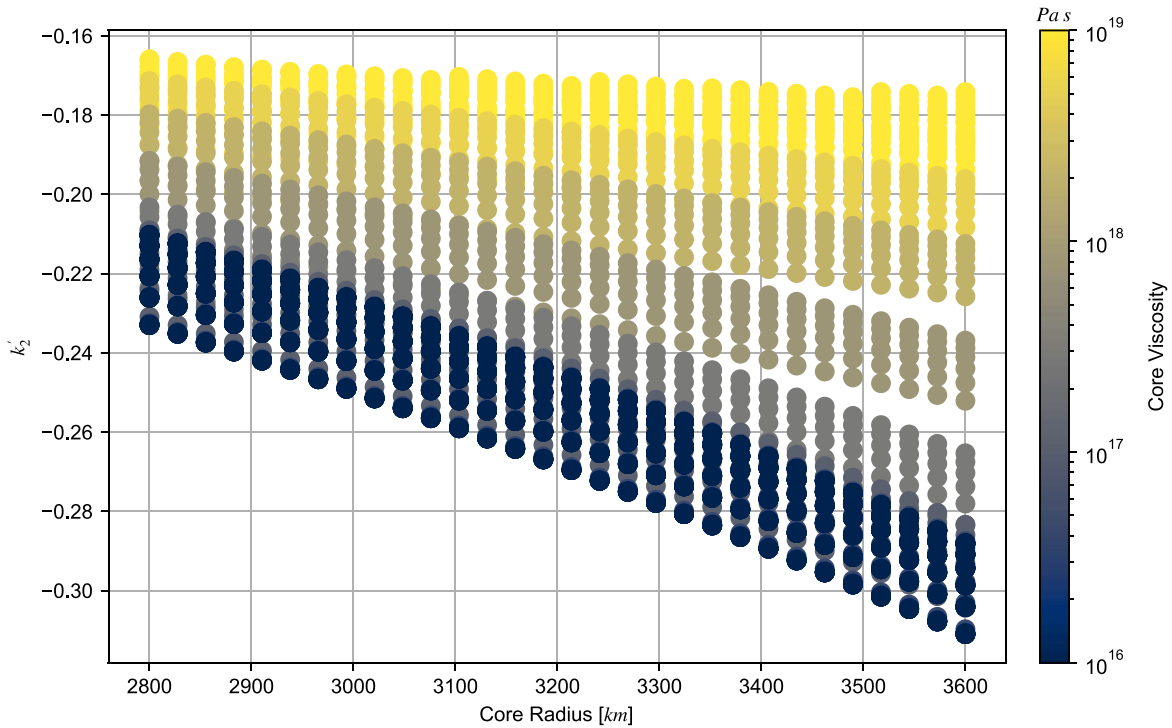


Figure 7. Degree 2 load Love number of Venus for models with a solid core and varying core size and viscosity.

load Love number. A purely elastic model of the interior would provide k_2' between -0.277 and -0.200 , discarding models with a solid core.

The observation of the degree 2 load Love number can be used to determine the state of the planetary core. Considering only the models that provide a tidal Love number k_2 in a range in agreement with the measurements (i.e., 0.210 – 0.395 ,

accounting for 3σ reported in Konopliv et al. 1999), we obtain k_2' between -0.340 and -0.210 for models with a fully liquid core and -0.305 and -0.165 for models with an entirely solid core. A high value of k_2' (larger than -0.210) would suggest the presence of a solid and highly viscous core (viscosity greater than $\sim 10^{18}$ Pa s). A value of k_2' lower than -0.305 should indicate that the core of Venus is fluid.

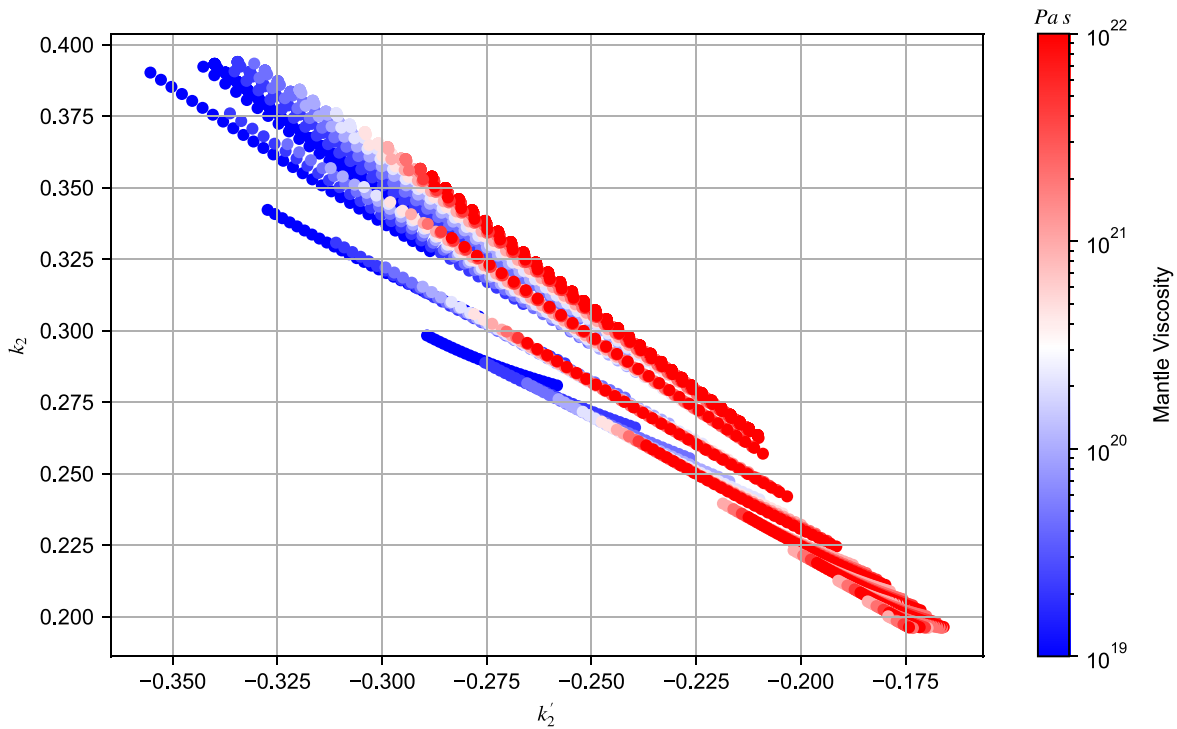


Figure 8. Degree 2 tidal and load Love numbers of Venus for all of the accepted models. The models are color-coded according to the viscosity of the mantle.

In addition to the possibility of discriminating between a solid and a liquid core, the load Love number k'_2 could be combined with the tidal Love number k_2 to constrain the properties of the internal layers. Figure 8 shows the pair of Love numbers k'_2 and k_2 for all of the models fulfilling the constraints given by the observed k_2 , MoI and mass.

The combination of these two parameters can significantly constrain the viscosity of the mantle, providing a complementary measurement to the value that could be inferred from observations of the gravitational tides phase lag (Dumoulin et al. 2017). A large absolute value of both the tidal and load Love numbers (i.e., $k_2 > 0.325$ and $k'_2 < -0.3$) would indicate a low mantle viscosity, whereas lower values ($k_2 < 0.275$ and $k'_2 > -0.225$) are characteristic of models with a highly viscous mantle. The resulting pairs of Love numbers k'_2 and k_2 for all of the models show an approximated linear trend whose best fit is given by $k'_2 = -0.798 k_2 - 0.013$.

3.2.2. Mars

Accurate measurements of the tidal Love number k_2 constraining Mars' deep interior suggest that its iron core is not entirely solid (Yoder et al. 2003; Rivoldini et al. 2011; Genova et al. 2016; Konopliv et al. 2016). The recent findings of the seismological investigation of the Mars InSight mission (Banerdt et al. 2020) provided refined constraints on the crust (Knapmeyer-Endrun et al. 2021), mantle (Khan et al. 2021), and core (Stähler et al. 2021) of the planet. Stähler et al. (2021) estimated the radius of the liquid core to be in the range 1830 ± 40 km. A solid inner core has not been detected yet. For this reason, our analysis is focused on models with an entirely fluid core that have a size consistent with three standard deviations of the InSight estimate (1710–1950 km). The rheology of the mantle is modeled as the Venus case. The crust is assumed to be elastic, with a constant mean bulk density of 2582 kg m^{-3} (Goossens et al. 2017a, 2017b) and an

average thickness of 42 km. The low-degree gravity field and Love numbers are not significantly affected by the crustal structure; therefore, we do not vary the properties.

Figure 9 shows the load Love numbers of Mars up to harmonic degree 20 for different interior models. Figure 9(a) illustrates the sensitivity of the load Love numbers on the mantle viscosity with the core radius fixed at 1830 km, while Figure 9(b) shows the effects of the core radius (mantle viscosity equal to 10^{20} Pa s).

As in the Venus case, the effects of the core size are limited to the lowest degrees of the harmonic expansion ($l < 5$), while the viscosity of the mantle also has a large effect at higher degrees. The sensitivity to the mantle viscosity is higher when compared to the Venus case because of the longer period of the mass redistribution on Mars (687 days of the CO_2 cycle compared to ~ 117 days of Venus's thermal tides). The lower frequency of the surface loading on Mars implies a greater dependence of the load Love numbers on the viscous dissipation within the mantle.

The higher accuracy of the determination of Mars' interior structure compared to Venus yields a significant constraint on the resulting load Love numbers k'_2 that ranges between -0.133 and -0.213 . Figure 10 shows k'_2 and k_2 for all of the models we generated.

In the case of Venus, the tidal and load Love numbers are characterized by similar sensitivity to the mantle viscosity, and the pairs k'_2 and k_2 show an approximate linear trend. Conversely, the load Love numbers of Mars are much more sensitive to the mantle viscosity than the tidal Love numbers. This is due to the large difference in the frequencies at which the Love numbers are computed (corresponding to ~ 12 hr and 687 days for the tidal and load Love numbers, respectively). The enhanced sensitivity to the viscous dissipation originated by the long period of the surface loading on Mars implies that the load Love numbers could play a crucial role in constraining

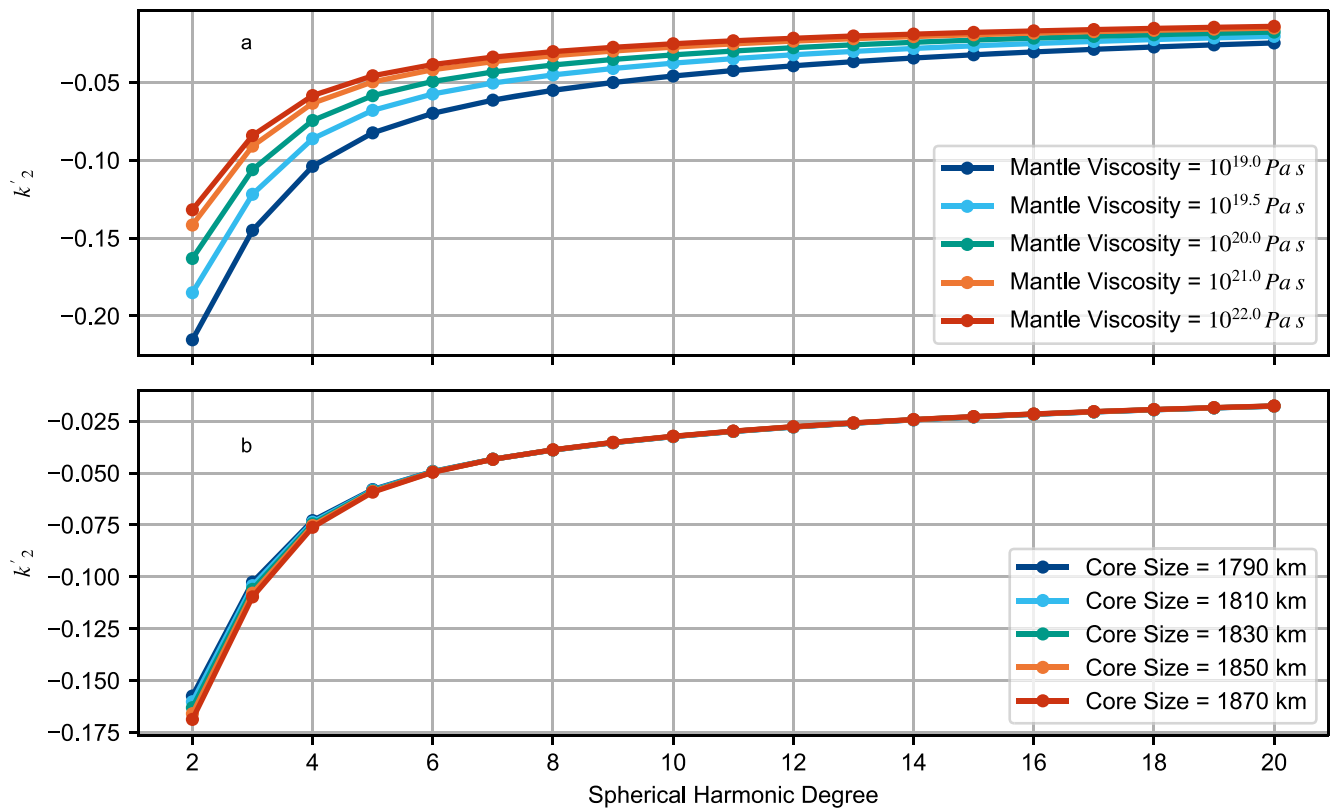


Figure 9. Load Love numbers of Mars up to degree 20 for different values of (a) mantle viscosity and (b) core radius.

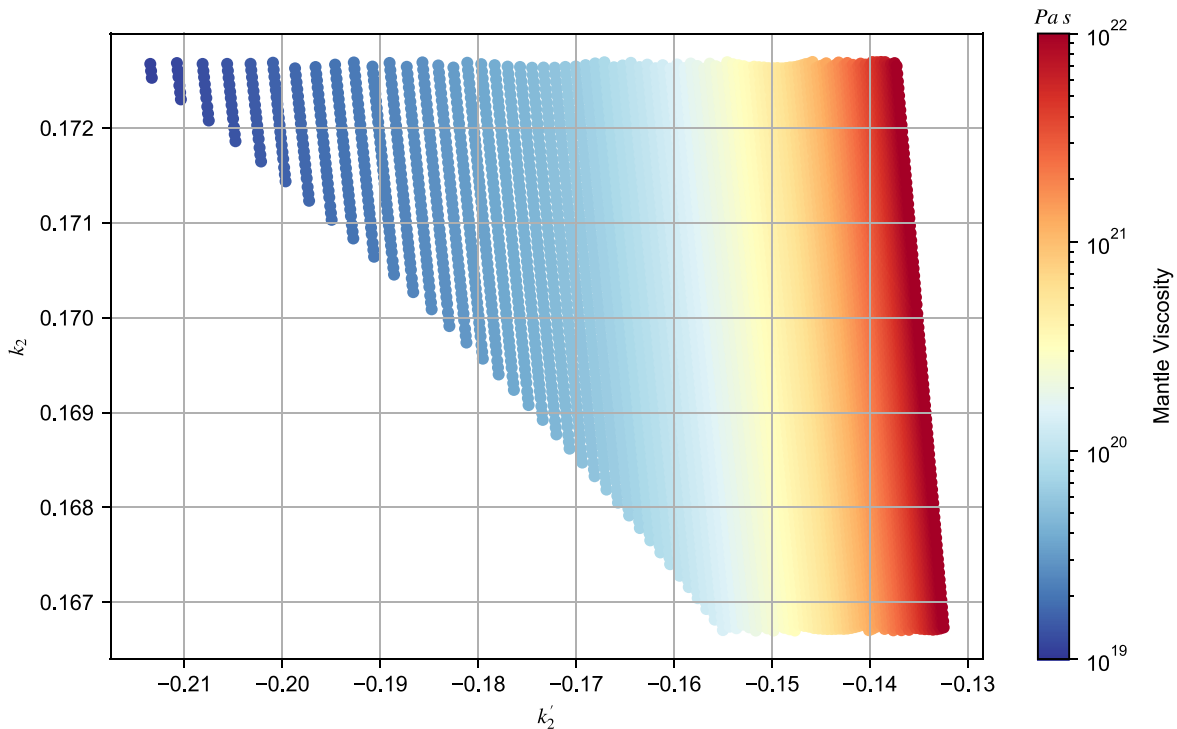


Figure 10. Degree 2 tidal and load Love numbers of Mars for all of the accepted models. The models are color-coded according to the viscosity of the mantle.

the interior structure. A high value of the degree 2 load Love number ($k'_2 > -0.16$) would indicate a highly viscous mantle, while lower values would suggest a low mantle viscosity.

Previous investigations (e.g., Karatekin et al. 2005; Sanchez et al. 2006) assumed that the effects of surface loading on Mars

are negligible because the available estimates of the magnitude of the load Love numbers were very small ($k'_2 \sim -0.05$). The refined constraints on the interior of Mars and the inclusion of viscoelastic effects in our modeling allow us to provide a more precise estimate of the load Love numbers. A better modeling

of the interior effects should be accounted for to accurately model the time-varying gravity field of Mars.

4. Discussion

Gravitational effects associated with the atmospheric dynamics preserve information on the interior of a celestial body because of the response to the loading deformations. In this work, we simulated the gravity field of Mars' and Venus' atmospheres and focused on the gravitational response to the surface pressure loading, measured by the load Love numbers. While the tidal Love numbers have been extensively investigated and used to constrain the inversion of the internal structure of planets and moons, the load Love numbers have been poorly explored. We investigated the interior response to the surface loading by generating internal structure models of Mars and Venus. The recent advancements in planetary rheological models allow us to include viscoelastic effects in our modeling, improving the estimates of the load Love numbers. The high sensitivity of the low-degree load Love numbers to the properties of the core and mantle implies that these parameters can significantly enhance the internal structure determination of celestial bodies that possess a surface fluid layer.

Measurements of Venus's k_2' can be used to discriminate between a solid ($k_2' > -0.210$) and liquid ($k_2' < -0.305$) core and constrain its size. In addition, the combination of the degree 2 tidal and load Love numbers may be employed to distinguish between a highly viscous mantle (i.e., viscosity $> 10^{21}$ Pa s if $k_2 < 0.275$ and $k_2' > -0.225$) and a low-viscosity mantle (i.e., viscosity $< 10^{20}$ Pa s if $k_2 > 0.325$ and $k_2' < -0.3$). An accurate estimate of these properties can greatly enhance the geological and thermal evolution modeling of Venus, leading to a better comprehension of the differences between the evolution of the Earth and Venus.

The load Love numbers can also provide crucial information on the interior structure in the case of Mars. The tidal Love number k_2 of Mars has been measured very accurately by gravity investigations (Genova et al. 2016; Konopliv et al. 2016). However, the gravitational tides phase lag, related to the imaginary part of k_2 and dependent on the dissipation within the mantle, has not been detected by these investigations. The tidal lag has been measured by observing Phobos's secular acceleration induced by gravitational tides and employed to infer the viscosity of the mantle (Bills et al. 2005; Jacobson 2010). An independent estimation of the mantle viscosity can be obtained through gravity investigations by combining the observations of the degree 2 tidal and load Love numbers.

The aim of future geophysical investigations across the solar system will be the determination of the interior structure of celestial bodies through the combination of different geophysical parameters. Love numbers can provide significant constraints on the inversion of internal structure from geodetic observations. The combination of different data sets, like those acquired by radio science, altimetry, and imaging, will be used to determine the tidal Love numbers k , h , and l , respectively. In this work, we also showed that the load Love number k' yields crucial information on the properties of celestial bodies' interiors and that its measurement will provide a further constraint on the determination of the internal structure. In addition, the combination of the potential tidal and load Love numbers k and k' offers the opportunity of indirectly

determining the amplitude of the radial deformations associated with the gravitational tides (see Equation (7)), providing an independent observation of the tidal Love number h . Therefore, the measurement of the load Love number k' can significantly extend the scientific return of geophysical investigations of planetary bodies and improve the determination of their interior structure.




5. Summary

In this study, we have investigated the gravity field of the terrestrial planets' atmospheres and provided details on their characteristics. We have also emphasized the existence of a coupling between this time-varying gravity field and the internal structure of the planet generated by the gravitational response to the atmospheric pressure loading on the surface and measured by the load Love numbers. We showed that the low-degree load Love numbers are particularly sensitive to the state, radius, and viscosity of the core and the viscosity of the mantle. An interior structure including a large fluid core is characterized by a high magnitude of the load Love numbers, while a small solid core leads to lower magnitudes. The viscosity of the core and mantle influences the interior response in a similar way, increasing the load Love numbers for low values of the viscosity. Given this sensitivity on the internal structure, the determination of the load Love numbers' contribution to the time-varying gravity field and their combination with the tidal Love numbers would provide unprecedented constraints on the modeling of planetary interiors. In the next decade, Venus will be explored by three different missions: the Deep Atmosphere Venus Investigation of Noble gases, Chemistry and Imaging (DAVINCI), EnVision, and the Venus Emissivity, Radio Science, InSAR, Topography, and Spectroscopy (VERITAS). VERITAS and EnVision are expected to yield great improvements in the determination of Venus's gravity field, providing a unique opportunity to detect for the first time Venus's time-varying gravity field and load Love numbers. To enable an independent estimation of the tidal and load Love numbers, the proposed modeling of the gravitational response associated with the atmospheric loading will be integrated in the precise orbit determination software as time-varying gravity field coefficients. By computing the partial derivatives of these time-varying coefficients with respect to the load Love numbers, we will be able to adjust this parameter in a global fit that includes the inversion of the static gravity field and the tidal Love number k_2 .

The spherical harmonics expansions and manipulations were performed with SHTools (Wieczorek & Meschede 2018). Some figures were produced with the Generic Mapping Tools (GMT; Wessel & Smith 1991). F.P. and L.I. are supported by the Italian Space Agency (ASI) under contract 2020-15-HH.0. F.P. and A.G. are grateful to Sébastien Lebonnois (Laboratoire de Météorologie Dynamique (LMD/IPSL), Paris) for his help with the setup of the Venus IPSL GCM and helpful discussions on Venus thermal tides. The contribution from S.G. is based upon work supported by NASA under award No. 80GSFC21M0002 (UMBC/CRESST II).

ORCID iDs

Flavio Petricca  <https://orcid.org/0000-0002-6574-0507>
Antonio Genova  <https://orcid.org/0000-0001-5584-492X>

Sander Goossens  <https://orcid.org/0000-0002-7707-1128>
 Luciano Iess  <https://orcid.org/0000-0002-6230-5825>
 Giorgio Spada  <https://orcid.org/0000-0001-7615-4709>

References

- Andrade, E. N. 1910, *RSPS*, **84**, 1
- Bagheri, A., Khan, A., Al-Attar, D., Crawford, O., & Giardini, D. 2019, *JGRE*, **124**, 2703
- Baland, R. M., Tobie, G., Lefèvre, A., & Van Hoolst, T. 2014, *Icar*, **237**, 29
- Banerdt, W. B., Smrekar, S. E., Banfield, D., et al. 2020, *NatGe*, **13**, 183
- Bills, B., Neumann, G. A., Smith, D. E., & Zuber, M. T. 2005, *JGRE*, **110**, E07004
- Bills, B., Navarro, T., Schubert, G., Ermakov, A., & Górski, K. M. 2020, *Icar*, **340**, 113568
- Blewitt, G. 2003, *JGRB*, **108**, 2103
- Boy, J. P., Gegout, P., & Hinderer, J. 2002, *GeoJI*, **149-2**, 543
- Boy, J. P., & Chao, B. F. 2005, *JGRB*, **110**, B08412
- Castillo-Rogez, J. C., Efroimsky, M., & Lainey, V. 2011, *JGR*, **116**, E09008
- Chao, B. F., & Gross, R. S. 1987, *GeoJI*, **91**, 569
- Davies, C. J., Stegman, D. R., & Dumberry, M. 2014, *GeoRL*, **41**, 3786
- Dumoulin, C., Tobie, G., Verhoeven, O., Rosenblatt, P., & Rambaux, N. 2017, *JGRE*, **122**, 1338
- Dziewonski, A., & Anderson, D. 1981, *PEPI*, **25**, 297
- Farrell, W. E. 1972, *RvGeo*, **10**, 761
- Garate-Lopez, I., & Lebonnois, S. 2018, *Icar*, **314**, 1
- Genova, A., Goossens, S., Lemoine, F. G., et al. 2016, *Icar*, **272**, 228
- Genova, A., Goossens, S., Mazarico, E., et al. 2019, *GeoRL*, **46**, 3625
- Genova, A. 2020, *AcAau*, **166**, 317
- Genova, A., & Petricca, F. 2021, *JGCD*, **44**, 1068
- Goossens, S., Lemoine, F. G., Rosenblatt, P., Lebonnois, S., & Mazarico, E. 2017a, *LPSC*, **48**, 1984
- Goossens, S., Sabaka, T. J., Genova, A., et al. 2017b, *GeoRL*, **44**, 7686
- Goossens, S., Mazarico, E., Rosenblatt, P., Lebonnois, S., & Lemoine, F. G. 2019, *LPI*, **2137**, 8029
- Hourdin, F., Le Van, P., Forget, F., & Talagrand, O. 1993, *JAtS*, **50**, 3625
- Iess, L., Jacobson, R. A., Ducci, M., et al. 2012, *Sci*, **337**, 457
- Jackson, I., & Faul, U. H. 2010, *PEPI*, **183**, 151
- Jacobson, R. A. 2010, *AJ*, **139**, 668
- James, P. B., Kieffer, H. H., & Paige, D. A. 1992, Mars (Tucson, AZ: Univ. Arizona Press), 934
- Justh, H. L., Justus, C. G., & Ramey, H. S. 2011, in The Fourth International Workshop on the Mars Atmosphere: Modelling and Observation, ed. F. Forget et al. (Paris: Pierre and Marie Curie Univ.), 265
- Karatekin, Ö., Duron, J., Rosenblatt, P., et al. 2005, *JGR*, **110**, E06001
- Kaula, W. M. 1963, Theory of Satellite Geodesy: Applications of Satellites to Geodesy (New York: Dover Publications)
- Khan, A., Ceylan, S., Van Driel, M. et al. 2021, *Sci*, **373**, 434
- Khan, A., Liebske, C., Rozel, A., et al. 2018, *JGRE*, **123**, 575
- Khan, A., Mosegaard, K., Williams, J. G., & Lognonné, P. 2004, *JGRE*, **109**, E09007
- Knapmeyer-Endrun, B., Panning, M. P., Bissig, F., et al. 2021, *Sci*, **373**, 438
- Konopliv, A. S., Asmar, S.W., Folkner, W. M., et al. 2011, *Icar*, **211**, 401
- Konopliv, A. S., Banerdt, W. B., & Sjogren, W. L. 1999, *Icar*, **139**, 3
- Konopliv, A. S., Park, R. S., Yuan, D. N., et al. 2013, *JGRE*, **118**, 1415
- Konopliv, A. S., Park, R. S., & Folkner, W. M. 2016, *Icar*, **274**, 253
- Konopliv, A. S., Park, R. S., & Ermakov, A. I. 2020, *Icar*, **335**, 113386
- Konopliv, A. S., & Yoder, C. F. 1996, *GeoRL*, **23**, 1857
- Lebonnois, S., Hourdin, F., Eymet, V., et al. 2010, *JGR*, **115**, E06006
- Lebonnois, S., Sugimoto, N., & Gilli, G. 2016, *Icar*, **278**, 38
- Leuliette, E. W., Nerem, R. S., & Russell, G. L. 2002, *JGRB*, **107**, 2112
- Lemoine, F. G., Goossens, S., Sabaka, T., et al. 2014, *GeoRL*, **41**, 3382
- Love, A. E. H. 1911, Some Problems of Geodynamics (New York: Dover)
- Margot, J.-L., Campbell, D. B., Giorgini, J. D., et al. 2021, *NatAs*, **5**, 676
- Mazarico, E., Genova, A., Goossens, S., et al. 2014, *JGRE*, **119**, 2417
- Metivier, L., Karatekin, O., & Dehant, V. 2008, *Icar*, **194**, 476
- Mitri, G., Meriggiola, R., Hayes, A., et al. 2014, *Icar*, **236**, 169
- Nimmo, F., & Faul, U. H. 2013, *JGRE*, **118**, 2558
- Padovan, S., Margot, J. L., Hauck, S. A., Moore, W. B., & Solomon, S. C. 2014, *JGRE*, **119**, 850
- Peltier, W. R. 1974, *RvGeo*, **12**, 649
- Reaman, D. M., Colijn, H. O., Yang, F., Hauser, A. J., & Panero, W. R. 2012, *E&PSL*, **349**, 8
- Renaud, J., & Henning, W. 2018, *ApJ*, **857**, 98
- Rivoldini, A., Van Hoolst, T., Verhoeven, O., Mocquet, A., & Dehant, V. 2011, *Icar*, **213**, 451
- Saito, M. 1974, *JPE*, **22**, 123
- Saito, M. 1978, *JPE*, **26**, 13
- Samuel, H., Lognonné, P., Panning, M., & Lainey, V. 2019, *Nature*, **569**, 523
- Sanchez, B. V., Rowlands, D. D., & Haberle, R. M. 2006, *JGR*, **111**, E06010
- Smith, D. E., Zuber, M. T., Haberle, R. M., Rowlands, D. D., & Murphy, J. R. 1999, *JGR*, **104**, 1885
- Spada, G., & Boschi, L. 2006, *GeoJI*, **166**, 309
- Spada, G. 2008, *CG*, **34**, 667
- Stähler, S. C., Khan, A., Banerdt, W. B., et al. 2021, *Sci*, **373**, 443
- Sundberg, M., & Cooper, R. 2010, *PMag*, **90**, 2817
- Takeuchi, H., & Saito, M. 1972, *Methods in Computational Physics: Advances in Research and Applications*, **11**, 217
- Tapley, B. D., Bettadpur, S., Watkins, M., & Reigber, C. 2004, *GeoRL*, **31**, L09607
- Van Orman, J. A. 2004, *GeoRL*, **31**, L20606
- Verma, A. K., & Margot, J.-L. 2016, *JGRE*, **121**, 1627
- Wahr, J., Molenaar, M., & Bryan, F. 1998, *JGR*, **103**, 30205
- Wahr, J., Swenson, S., Zlotnicki, V., & Velicogna, I. 2004, *GeoRL*, **31**, L11501
- Wessel, P., & Smith, W. H. F. 1991, *EOSTr*, **72**, 441
- Wieczorek, M. A., & Meschede, M. 2018, *GGG*, **19**, 2574
- Wilson, R. J., & Hamilton, K. 1996, *JAtS*, **53**, 1290
- Wouters, B., Bonin, J. A., Chambers, D. P., et al. 2014, *RPPH*, **77**, 116801
- Yoder, C. F., Konopliv, A. S., Yuan, D. N., Standish, E. M., & Folkner, W. M. 2003, *Sci*, **300**, 299